中國機械工程學刊第四十二卷第一期第 73~80 頁(民國一百一十年)
Journal of the Chinese Society of Mechanical Engineers, Vol.42, No.1, pp 73~80 (2021)

Research on Test for Phase Response Characteristics of VVT

Yin-guo Huang*, Xiao-long Luo**, Mei-rong Zhao,
Yi-cheng Wang, and Ye-long Zheng***

Key Words: VVT, Dynamic Test, Phase Response Characteristics, Engine Environment Simulation

ABSTRACT

Variable Valve Timing (VVT) in automotive engines regulates the phases of engine intake and exhaust at the right time, playing a vital role in improving power, fuel consumption, and emissions reduction. The optimization of the phase response characteristics in the VVT is an efficient way to optimize engine performances. For the purpose of the design and optimization of the VVT, the actual phase response characteristics must be obtained by the test of the VVT phase response characteristics. A VVT test system was designed and presented in this paper. To get the actual VVT phase response characteristics, a three-motor architecture was adopted in this test system, which simulating the actual and real working environment of the engine. In the test system, the driving motor (a three-phase induction motor) simulates the crank shaft of the engine, while the load motor (the permanent magnet synchronous machine, PMSM) is used as the cam shaft of the engine. And the Brushless Direct Current (BLDC) motor drives the VVT. If applying the conventional Proportional-Integral-Differential (PID) controller, the overshooting would be high and the regulating time was too long. With the nonlinear element added to the conventional PID, the defect was broken. It was highly proved through simulations and experiments that the VVT had a faster phase response and small overshooting using the proposed standardized nonlinear PID (SNPID).

Paper Received May, 2019. Revised Sepfember, 2019, Accepted October, 2019, Author for Correspondence: Ye-long Zheng

State Key Laboratory of Precision Measurement Technology and Instruments, School of Precision Instruments and Opto-Electronics Engineering, Tianjin University, Weijin Road 92, Nankai, Tianjin 300072, China.

**Associate Professor*
***Postgraduate student*
****Lecturer*

INTRODUCTION

VVT, a technology that varies the opening or closing time of engine valves, improves power, fuel consumption, and emissions reduction. As shown in Figure 1, VVT regulates the angle of the camshaft to advance or delay the opening or closing time of the valves, thus changing the air charge coefficient in the cylinders in every cycle and influencing the torque and power output (Ohsugi, A. et al, 2015). The number of valves may be two, four or five. However, to simplify the diagram, two valves are shown. Green represents the intake valve and red represents the exhaust valve. The time of opening or closing in advance or in a delaying way for valves, corresponding to the rotary angle of the camshaft is namely valve timing of the engine. The authors designed the engine VVT test system, which simulates the actual operating conditions of the BLDC in the engine and tests the dynamic performance of the VVT based on that system. The test was intended to optimize the dynamic phase response characteristics of VVT.

There are a variety of VVT systems, one of which is electrically driven. The principle of the electrically driven VVT is as follows: when the rotary speed of the BLDC is lower than that of the camshaft, valve timing is delayed, meaning that the opening or closing time of the valve is delayed. When the rotary speed of the BLDC is equal to the latter, valve timing maintains its original value. This means that the opening or closing time of the valve doesn't advance or delay. And when the rotary speed of the BLDC is higher than the latter, valve timing advances, meaning that the opening or closing time of the valve is advanced. Therefore, controlling the BLDC allows the opening or closing time of the valve to adjust and to regulate the time and airflow of the engine intake or exhaust. This, in turn, affects the capability of the engine.

The V-cycle is widely used in automotive control system development. It includes all functions from the determination of system requirements to system validation and approval. The hardware-in-the-loop (HIL) simulation is a part of the V-cycle function verification (Shugang, J. et al, 2009). The test, as well as the simulation of the real working environment of engine, presented in this paper, based on the VVT test system, is essentially an HIL simulation. Moreover, it functions as a BLDC-in-the-loop simulation.

MODEL OF THE TEST SYSTEM

To test the VVT, the authors designed a system that included both hardware and software subsystems. The structure and principle of the VVT test system are shown in Figure 2. The driving motor (a three-phase induction motor) simulates the crankshaft, and the load motor (a PMSM) simulates the camshaft. The goal of the test was to shorten the time of phase regulation, and decrease the overshooting as much as possible. Only when the VVT has a rapid response, small overshooting and phase stability, can it regulate and control the valve timing effectively and achieve optimum performance.

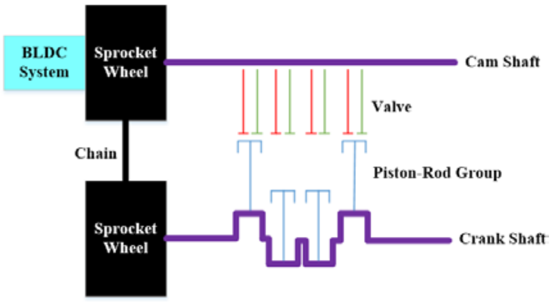

Fig. 1. Simplified Engine Diagram

The test system is actually a multi-motor control system essentially and the controlled devices are three motors: a BLDC, a PMSM, and a three-phase induction motor. Each motor has an independent control system to drive specific objects. However, these objects interact in a complicated way through a nonlinear coupling, which makes it more difficult to precisely control. From the standpoint of control requirements, a multi-motor system must control each motor independently. This means that not only every motor must perform well, but the nonlinear objects coupled with the motors must alleviate the effects of destabilization when the system is affected by unknown disturbances. When these are achieved the whole system functions at its optimum level (Liu, X. et al, 2013).

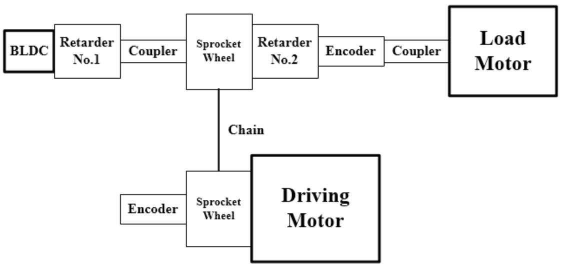

Fig. 2. Structure of the VVT Test System

During its practical application, the synchronism of the multi-motor system will deteriorate due to factors such as a mismatch between shafts and motors, and load disturbances (Cao, C. et al, 2013). Changfan Zhang, and Jing He, et al, implemented consensus tracking of the multi-motor system based on a variable structure approach. Their theoretical and simulated results illustrated the efficient performance of the proposed algorithm in terms of synchronization control accuracy, disturbance immunity, and convergence (Changfan, Z. et al, 2015). Taehyung Kim, and Kwang-Woon Lee, et al, proposed Dual Functional Control (DFC) to control two PMSMs in real-time, govern the energy storage system, and verify the feasibility of the control scheme via simulations and experiments (Taehyung, K. et al, 2015). Younes Sangsefidi and Saleh Ziaeinejad et al, proposed, based on a four-leg converter, a Direct Torque Control (DTC) of a two-phase induction motor (as the main motor) and hysteresis current control of a permanent magnet DC motor (as the auxiliary motor) (Younes, S. et al, 2015). They also recommended an augmented switching table to control both motors. Using theoretical analysis and experiments, this approach demonstrated. the capability of the system.

CONTROLLER MODELLING AND ANALYSIS

The rotary angle between the load shaft and driving shaft, is defined as the phase angle, and is the same as the valve timing of the engine. In Figure 2, the VVT phase is

$$\varphi = \int \omega_1 \mathrm{d}t - \int \omega_2 \mathrm{d}t \tag{1}$$

where ω_1 and ω_2 are the actual transient speed of the PMSM and driving motor, respectively. Using the same hardware clock, the host computer obtains speed values from encoders and calculates numerical integration to obtain phase values. To control the phase, the speed of the BLDC and load motor needs to be controlled respectively and synchronously. During the tests, the BLDC and load motor are controlled directly and the driving motor indirectly.

Assuming that the every phase of the BLDC is equivalent, the mathematical model of it is (Guocheng, C. et al, 2016):

$$\begin{cases} u_{\mathrm{v}} = e_{\mathrm{f}} + (\mathrm{L} - \mathrm{M})\dfrac{\mathrm{d}i}{\mathrm{d}t} + i\mathrm{R} \\ e_{\mathrm{f}} = \mathrm{K}_{\mathrm{e}}\omega_3 \\ T_{\mathrm{e}} - T_{\mathrm{L}} - \mathrm{f}_{\mathrm{f}}\omega_3 = \mathrm{J}_3\dfrac{\mathrm{d}\omega_3}{\mathrm{d}t} \\ T_{\mathrm{e}} = \mathrm{K}_{\mathrm{T}}i \end{cases} \tag{2}$$

where u_{v} is the phase voltage, i is the current, e_{f} is the induced electromotive force, L is the self-inductance coefficient, M is the mutual inductance coefficient, R is the equivalent resistance, K_e is the electromotive force coefficient, ω_3 is the speed of the BLDC, T_e is the output torque, T_L is the load torque, f_f is the friction coefficient, J_3 is the rotor inertia of the BLDC, and K_T is the torque coefficient. The PWM frequency is controlled to regulate the speed of the BLDC and to control the rotary angle, thus reducing reliance on the inherent parameters of the BLDC, and satisfying the requirements for engineering accuracy.

The mathematical model of the load motor (Sarayut, A. et al, 2015) is

$$\begin{cases} u_d = R_s i_d + L_d \dfrac{d}{dt} i_d - \omega_e L_q i_q \\ u_q = R_s i_q + L_q \dfrac{d}{dt} i_q + \omega_e L_d i_d + \omega_e \lambda_m \\ T_{Pe} = \dfrac{3}{2} p(\lambda_d i_q - \lambda_q i_d) \\ J_1 \dfrac{d\omega_1}{dt} = T_{Pe} - T_{PL} - B\omega_1 \end{cases} \tag{3}$$

where u_d and u_q are the stator voltages of the d axle and q axle, respectively. The terms i_d and i_q are stator currents of the d axle and q axle, respectively. R_s is stator resistance. The terms λ_d and λ_q are stator flux linkages of the d axle and q axle respectively. The terms ω_e and ω_1 are the electrical angular speed and rotor angular speed, respectively. The terms L_d and L_q are the inductances of the d axle and q axle respectively. The term λ_m is the rotor PM flux linkage. The terms T_{Pe} and T_{PL} are the electromagnetic torque and the load torque of the load motor, respectively. The term p is the number of pole pairs, B is the friction coefficient, and J_1 is the moment of inertia of the rotor and load.

The mathematical model of the VVT test system is

$$J_1 \frac{d\omega_1}{dt} + J_2 \frac{d\omega_2}{dt} + J_3 \frac{d\omega_3}{dt} + J_4 i_2 \frac{d\omega_1}{dt} + J_5 \frac{i_2 d\omega_1}{dt} + f_1\omega_1 + f_2\omega_2 + f_3 i_1 i_2 \omega_1 = T_d + T_e - T_{Pe} \tag{4}$$

$$\omega_3 = i_1 i_2 \omega_1 \tag{5}$$

where J_2 and ω_2 are the rotor moment of inertia and angular speed of driving motor, J_4 is the moment of inertia of the retarder No.1 rotor, i_2 is the coupler close to the BLDC and the reduction ratio of the retarder No.2. The term J_5 is the moment of inertia of retarder rotor and coupler close to the load motor. The term i_1 is the reduction ratio. The terms f_1, f_2, and f_3 are friction coefficients. The term T_d is the output torque of the driving motor. Using the converter, the auto tuning of the driving motor recognizes the parameters of the motor and the system such as double-loop PID increases of the speed loop and current loop, the total moment of inertia, and friction coefficients. Using the servo motor controller, the speed and output torque of the load motor are controlled directly. Controlling the speed of BLDC makes it possible to track the speed of the driving motor. Then the speed of the synchronous control is determined while controlling the phase of the VVT at the same time.

Though the conventional PID controller may be used to control the speed of the motors, the performance of rapid responses of the machine under changing loads cannot be ensured (Gunapriya, B. et al, 2017). Researchers and engineers tend to improve the conventional PID controller or propose other algorithms to achieve better control system performance rather than using the PID directly, such as adopting the fuzzy neural technique to control the BLDC speed (Chen, P. et al, 2016). However, the fuzzy neural technique may be too complex and costly to achieve. To optimize the performance of the system, the authors of this paper inserted a nonlinear unit before the proportional part of the PID controller. The control system is essentially nonlinear and inserting a nonlinear unit can improve the performance of rapid phase response. The equivalent transformation from the proportional component and the nonlinear unit in series to a new nonlinear unit makes it possible that the equivalent nonlinear unit can be regulated in real-time. The time-domain expression of the equivalent nonlinear unit is

$$K(t) = K_p[\frac{e(t)}{c} - 1]^2 \tag{6}$$

where $K(t)$ is the equivalent nonlinear unit, $e(t)$ is the phase error, c is a constant, and K_p is the proportional gain of the traditional PID controller. When the constant c in Equation (6) is set to different values the control system will be going to different dynamic performances.

During the process of controlling the nonlinear time-variable coupling of objects, once parameters are set they can't be adjusted online and in real-time. Moreover, the anti-interference and the performance of response is poor (Cui, J. et al, 2013). As shown in Equation (6), the authors designed the SNPID to fill the gap with a nonlinear element added to the conventional PID controller. Simultaneously, the synchronous tracking performance improved along with the control accuracy of the phase.

Assuming that the input and output of the PID controller are $u(t)$ and $y(t)$, respectively, the PID control law is shown below:

$$\begin{aligned} y(t) &= K_p[\frac{e(t)}{c} - 1]^2 + K_i \int e(t)dt + K_d f(t) \\ &= K_p[\frac{u(t)-y(t)}{c} - 1]^2 + \\ &\quad K_i \int [u(t) - y(t)]dt + K_d f(t) \end{aligned} \tag{7}$$

where K_p, K_i, K_d are the PID gains, $e(t)$ is the error between $u(t)$ and $y(t)$, and $f(t)$ is the product of a differential element and an inertial element. The transfer function is

$$G(s) = \frac{F(s)}{E(s)} = \frac{s}{s+1} \tag{8}$$

Therefore, the Laplace Transformation of f(*t*) is

$$F(s) = G(s)E(s) = \frac{s}{s+1}E(s) \tag{9}$$

where *E(s)* is the the Laplace Transformation of *e*(*t*). The time-domain expression of Equation (9) is

$$\frac{\mathrm{d}f(t)}{\mathrm{d}t} + f(t) = \frac{\mathrm{d}e(t)}{\mathrm{d}t} \tag{10}$$

Solving the differential equation, *f*(*t*) is

$$f(t) = e^{-t}\left(\int \frac{\mathrm{d}e(t)}{\mathrm{d}t} e^{t}\mathrm{d}t + a_0\right) \tag{11}$$

where e^{-t} and e^{t} are exponential functions of time t, and a_0 is the initial constant of the differential equation. Assuming that *y*(*t*) is second-order continuous differentiable and the the initial constant a_0 equals to zero, the initial state is

$$y(0) = \mathrm{K_p}\left[\frac{u(0)-y(0)}{\mathrm{c}} - 1\right]^2 \tag{12}$$

which means that the initial state is determined by the constant c and $\mathrm{K_p}$, and the derivative of *y*(*t*) is

$$\begin{aligned}\frac{\mathrm{d}y}{\mathrm{d}t} &= -\frac{2\mathrm{K_p}}{\mathrm{c}}\left(\frac{u-y}{\mathrm{c}} - 1\right)\frac{\mathrm{d}y}{\mathrm{d}t} + \\ &\mathrm{K_i}(u-y) + \mathrm{K_d}e^{-t}\int \frac{\mathrm{d}y}{\mathrm{d}t}e^{t}\mathrm{d}t - \mathrm{K_d}\frac{\mathrm{d}y}{\mathrm{d}t}\end{aligned} \tag{13}$$

where *u* is the input of the step signal. Therefore, the the derivative of *u*(*t*) is zero. The second-order derivative of *y*(*t*) is

$$\begin{aligned}\frac{\mathrm{d}^2y}{\mathrm{d}t^2} &= \frac{2\mathrm{K_p}}{\mathrm{c}^2}\left(\frac{\mathrm{d}y}{\mathrm{d}t}\right)^2 - \frac{2\mathrm{K_p}}{\mathrm{c}}\left(\frac{u-y}{\mathrm{c}} - 1\right)\frac{\mathrm{d}^2y}{\mathrm{d}t^2} \\ &-\mathrm{K_i}\frac{\mathrm{d}y}{\mathrm{d}t} - \mathrm{K_d}e^{-t}\int e^{t}\mathrm{d}y + \mathrm{K_d}\frac{\mathrm{d}y}{\mathrm{d}t} - \mathrm{K_d}\frac{\mathrm{d}^2y}{\mathrm{d}t^2}\end{aligned} \tag{14}$$

Equation (14) is transformed as

$$\begin{aligned}&\left[1 + \frac{2\mathrm{K_p}}{\mathrm{c}}\left(\frac{u-y}{\mathrm{c}} - 1\right) + \mathrm{K_d}\right]\frac{\mathrm{d}^2y}{\mathrm{d}t^2} \\ &= \frac{2\mathrm{K_p}}{\mathrm{c}^2}\left(\frac{\mathrm{d}y}{\mathrm{d}t}\right)^2 - \mathrm{K_i}\frac{\mathrm{d}y}{\mathrm{d}t} - \mathrm{K_d}e^{-t}\int e^{t}\mathrm{d}y + \mathrm{K_d}\frac{\mathrm{d}y}{\mathrm{d}t}\end{aligned} \tag{15}$$

To simplify Equation (15), it is written as

$$\square \frac{d^2y}{dt^2} = g \tag{16}$$

If *h* is larger than zero and *g* smaller than zero, the second-order derivative of *y*(*t*) is smaller than zero, and the derivative of *y*(*t*) monotonically decreases, thus *y*(*t*) converging. Therefore, c should be set at a large value to make *y*(*t*) converge. On the contrary, if *y*(*t*) diverges, the overshooting is a serious and dangerous phenomenon. In conclusion, the constant c is one of the dominant elements for the dynamic performances of the system.

When *y*(*t*) is in a steady state, the steady state response is

$$y_s = \mathrm{K_p}\left[\frac{e_s}{\mathrm{c}} - 1\right]^2 + \mathrm{K_i}\int e(t)\mathrm{d}t + \mathrm{K_d}f(t) \tag{17}$$

where y_s and e_s represent the steady-state response and the steady state error, respectively. Equation (17) demonstrates that e_s, c, $\mathrm{K_p}$, $\mathrm{K_i}$, and $\mathrm{K_d}$ together determine the steady state response.

Setting the step signal, $\mathrm{K_p}$, $\mathrm{K_i}$, and $\mathrm{K_d}$ at 10, 5, 50, and 0.1, respectively, the simulation of the SNPID and the conventional PID controller are as follows. Comparing Figure 4 with Figure 5, obviously, the SNPID controller has a faster dynamic response than the latter. If the constant c is greater than 1, it means that the error is reduced. When c is set to appropriate values such as 150 or 80, the algorithm converges at a rapid pace, which means that the performance of rapid response is exceptional. Figure 6 shows that some values of c lead to divergence of the algorithm, which means that an improper value of c leads to unstable states of the system. Figure 3 shows the dynamic *K*(*t*) in the equation (6) in which -1 makes *K*(*t*) approaches $\mathrm{K_p}$ while *e*(*t*) is close to zero.

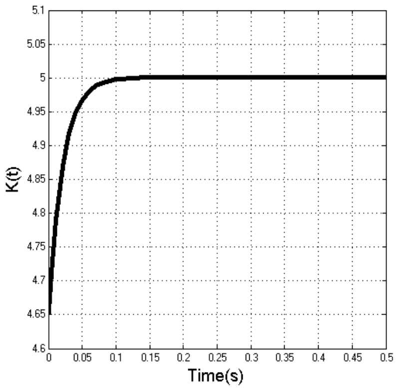

Fig. 3. K(t) Values

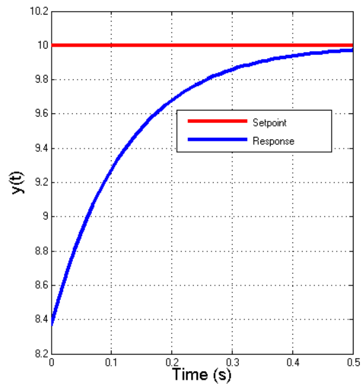

Fig. 4. Step Signal and Response of the Conventional PID

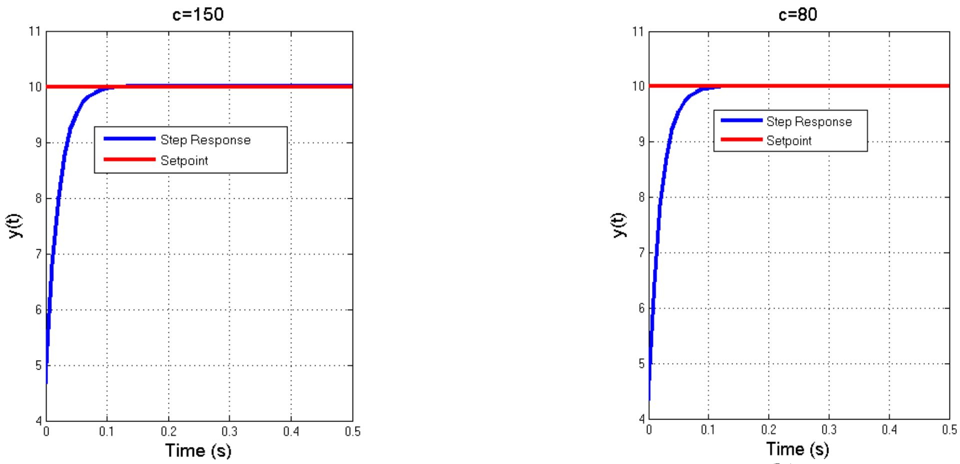

(a) (b)

Fig. 5. Step Signal and Response of the SNPID

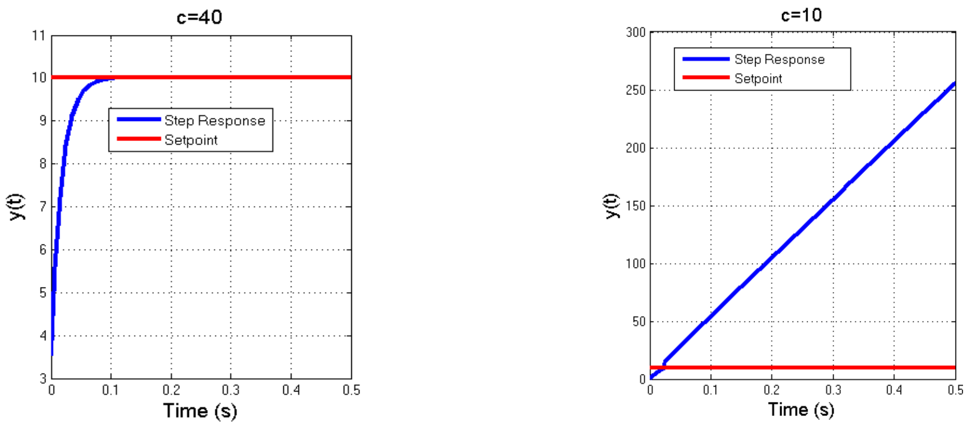

(a) (b)

Fig. 6. Step Signal and Response of the SNPID

Equation (9) includes a derivative element and an inertia element. The simulation results shown in Figure 4, 5 and 6(a), make it clear that the overshooting of the system is extremely small. And the nonlinear element makes the system regulate more rapidly.

The limitation of c is that it is not a tunable parameter, which means that the proposed nonlinear PID controller is not a truly adaptive PID. If c varies in real-time, the proposed standardized nonlinear PID would be adaptive and simultaneously the algorithm complexity would rise. But c has a negligible impact on the dynamic performance of the system, in a large range of c while changing it. What's more, inappropriate values of c may lead to divergence. In general, the more numerous the variables are, the more sophisticated the PID controller is. Omer Saleem and Urwa Omer (Omer, S. et al, 2017), who defined PI controller gains as the functions of the error and the derivative of the error, presented a robust adaptive nonlinear proportional-integral (ANPI) scheme to control the speed of a direct-current motor. Actually it is further more complex than the SNPID of this paper. If the complexity of algorithms is too high, the system responses will not be fast.

All in all, the SNPID algorithm both has advantages and disadvantages. In different application scenarios, the requirements vary. The most important is the choice and design of proper algorithms according to different requirements and conditions.

EXPERIMENTS AND ANALYSIS

The VVT facilitates extended adaptation to different operating conditions, from which numerous benefits are derived, including higher rated power, and improved operation at low engine speeds, etc (Konrad, R. et al, 2015). The authors choose several typical speeds at the low range, such as 1000rpm and 1500rpm, etc. In this paper, the time between sending the instruction to regulate the phase to a variation of 10° is defined as the ascending time or descending time, and the time between sending the instruction to regulate the phase to the stable state (in the range of ±5% of the setpoint) is defined as the adjusting time. With the SNPID, the experimental results are as follows.

When the speed of BLDC is 1000rpm, the phase regulation curve is that shown in Figure 7. In all of the phase regulation diagrams, the left vertical axis indicates the PWM duty ratio, phase setpoint, and actual phase. The right axis shows the speed of the BLDC. With the phase ascending from 20° to 30°, the ascending time is 355.16ms, and the adjusting time is 374.32ms. If the speed of the BLDC is adjusted to increase it, a peak appears in the blue curve, indicating the moment the phase rises. If the BLDC is reversed to decrease the speed, the duty ratio, displayed with a green curve, drops from 80% to 30%. This is shown in the blue curve, indicating that the phase descends.

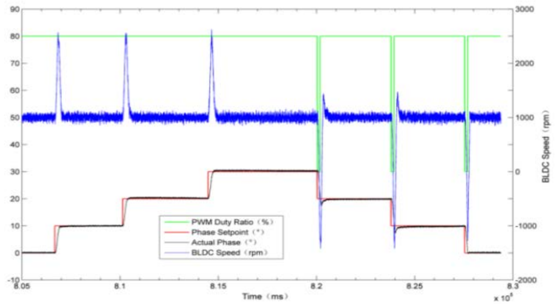

Fig. 7. Phase Regulation Curve. When BLDC Speed is 1,000rpm. The left axis represents the PWM duty ratio, phase setpoint, and actual phase, and the right axis shows the BLDC speed.

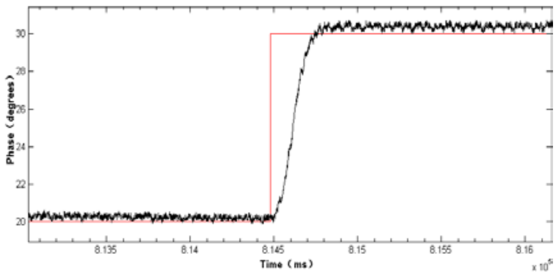

Fig. 8. Partial Enlarged Detail of Figure 7. When the speed of the BLDC is 1,500rpm, the phase regulation curve is that shown in Figure 9. With the phase ascending from 20° to 30°, the ascending time is 300.38ms, and the adjusting time is 320.49ms.

When the speed of the BLDC is 2,500rpm, the phase regulation curve is as shown in Figure 11. With the phase ascending from 20° to 30°, the ascending time is 415.52ms, and the adjusting time is 432.63ms.

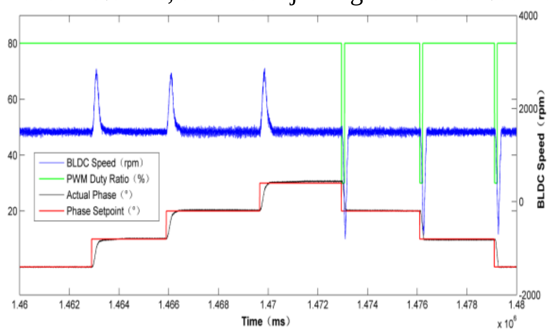

Fig. 9. Phase Regulation Curve. When the BLDC Speed is 1,500rpm. The left axis represents the PWM duty ratio, phase setpoint, and actual phase, and the right axis shows the BLDC speed.

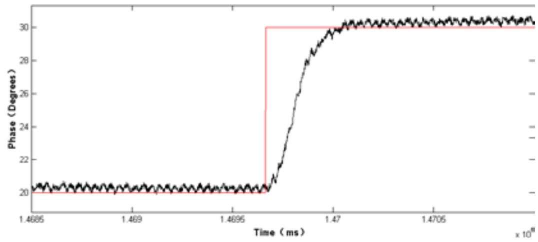

Fig. 10. Partial Enlarged Detail Figure 9

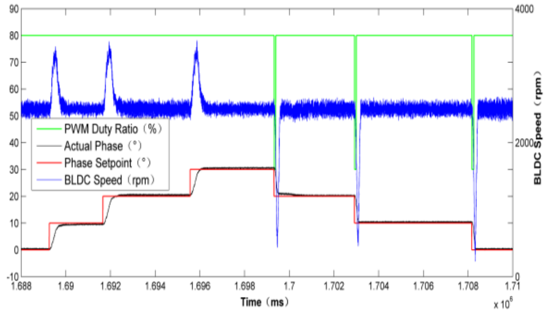

Fig. 11. Phase Regulation Curve. When BLDC Speed is 2,500rpm. The left axis represents the PWM duty ratio, phase setpoint, and actual phase, and the right axis shows the BLDC speed.

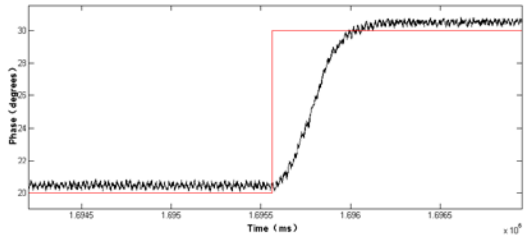

Fig. 12. Partial Enlarged Detail Figure 11. When the speed of BLDC is 3,000rpm, the phase regulation curve is as shown in Figure 13. With the phase ascending from 20° to 30°, the ascending time is 791.73ms, and the adjusting time is 808.37ms.

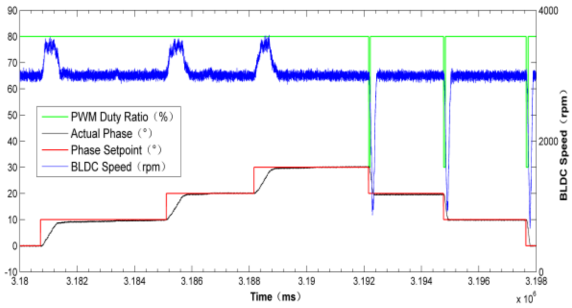

Fig. 13. Phase Regulation Curve. When the BLDC Speed is 3,000rpm. The left axis represents the PWM duty ratio, phase setpoint, and actual phase, and the right axis shows the BLDC speed.

For comparison, only the ascending time and the adjusting time from 20° to 30° of the phase are listed in Table 1 and Table 2, which reveals the significant differences. The apparent is that the ascending time and the adjusting time are different when the PID gains and constant c change, as do the dynamic characteristics of the VVT.

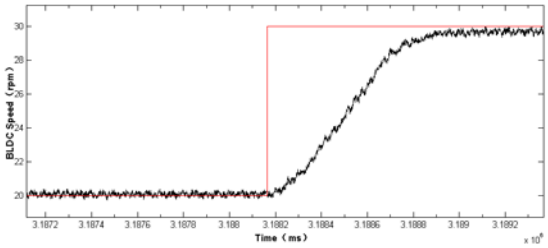

Fig. 14. Partial Enlarged Detail Figure 13

Table 1. Response Time of the VVT Phase With the Conventional PID

BLDC speed (rpm)	Ascending Time (ms)	Adjusting Time (ms)
1,000	453.23	1,250.33
2,000	255.47	1,403.48
3,000	713.62	2,689.83

Table 2. Response Time of the VVT Phase With the SNPID

BLDC speed (rpm)	Ascending Time (ms)	Adjusting Time (ms)
1,000	355.16	374.32
1,500	300.38	320.49
2,500	415.52	432.63
3,000	791.73	808.37

CONCLUSIONS

To test the VVT phase response characteristics, the program above was designed. The test of VVT phase response characteristics was performed through the simulation of the actual and real working environment of engine, with the multi-motor control. In the triple-motor system, the driving motor (a three-phase induction motor) simulates the crank shaft of the engine, while the the load motor, namely the PMSM, simulates the cam shaft of the engine. And the BLDC motor in the test system drives the VVT. The types and the characteristics of the three motors are different, and the features of multi-variable, strong coupling and non-linearity, etc (Minlin, W. et al, 2018), make it much harder to control the multi-motor system accurately and synchronously. In this test system including the three motors mentioned above, the overshooting was high and the regulating time was too long, with the conventional PID controller. However, it was highly proved through simulations and experiments that the VVT was provided with the faster phase response using the SNPID, and at the same time, the overshooting of the VVT phase was minimal.

CONFLICT OF INTEREST

The authors declare no conflicts of interests.

ACKNOWLEDGEMENT

This work is supported by the National Natural Science Foundation of China (Grant No. 51425502) and Tianjin Natural Science Foundation (No. 18JCQNJC04800, 18JCZDJC31800 and 18JCYBJC16100).

REFERENCES

Cao, C., Wang, B., and Xu, X., "Research On Relative Coupling Control for Multi-motor Synchronization Based on Neural Network," Control Engineering of China, Vol. 20, No. 3, pp. 415-418, (2013).

Changfan, Z., Han, W., and Jing, H., "Consensus tracking for multi-motor system via observer based variable structure approach," Journal of the Franklin Institute, Vol. 352, No. 8, pp. 3366-3377, (2015).

Chen, P., "BLDC Motor Speed Control Using Fuzzy Neural Technique," Journal of the Chinese Society of Mechanical Engineers, Vol. 37, No. 6, pp. 567-576, (2016).

Cui, J., Liu, Y., and Yan, H., "Multi-motor Neuron PID Synchronous Control Based on Fuzzy Control," Modular Machine Tool & Automatic Manufacturing Technique, No.2, pp. 81-83+87, (2013).

Gunapriya, B. and Sabrigiriraj, M., "Real-Time Implementation and Performance Evaluation of Brain Emotional Learning Developed for FPGA-Based PMBLDC Motor Drives," Journal of Testing and Evaluation, Vol. 45, No. 3, pp. 987-1004, (2017).

Guocheng, C., "PWM Patterns and Power Electronic Conversion Technologies," China Electric Power Press, Beijing, pp. 117-145, (2016).

Konrad, R., "Gasoline Engine Management: Systems and Components," Springer Fachmedien Wiesbaden, Wiesbaden, Germany, pp. 32-49, (2015).

Liu, X., Guan, P., and Liu, L., "Certain problems for robust adaptive control on a class of multi-motor system," Journal of Beijing Information Science and Technology University, Vol. 28, No. 1, pp. 5-12, (2013).

Minlin, W., Xuemei, R., and Qiang, C., "Robust tracking and distributed synchronization control of a multi-motor servomechanism with H-infinity performance," ISA Transactions, No. 72, pp. 147-160, (2018).

Ohsugi, A., Toyoda, M., and Tielong, S., "Optimal calibration of VVT by extremal seeking in combustion engines," 54th Annual Conference of the Society of Instrument and Control Engineers of Japan (SICE), pp. 1337-1340, Hangzhou, (2015).

Omer, S., and Urwa, O., "EKF-based self-regulation of an adaptive nonlinear PI speed controller for a DC motor," Turkish Journal of Electrical Engineering & Computer Sciences, No. 25, pp. 4131-4141, (2017).

Sarayut, A., Mongkol, E., and Nattapon, C., "A single chip FPGA-based solution for controlling of multi-unit PMSM motor with time-division multiplexing scheme," Microprocessors and Microsystems, Vol. 39, No. 8, pp. 621-633, (2015).

Shugang, J., Michael, H. S., and Atsushi, O., "Development of an Engine-in-the-loop Vehicle Simulation System in Engine Dynamometer Test Cell," SAE International, USA, (2009).

Taehyung, K., Kwang-Woon, L., and Sangshin, K., "Multi Motor Drive Based on a Dual Purpose DC-DC Power Conversion System," The Seventh Annual IEEE Energy Conversion Congress and Exposition (ECCE 2015) , pp. 4048- 4054, Montreal, (2015).

Younes, S., Saleh, Z., and Ali, M., "A New Two-Motor Drive to Control a Two-Phase Induction Motor and a DC Motor," 2015 IEEE International Electric Machines & Drives Conference (IEMDC), pp. 818-822, Coeur d'Alene, (2015).

VVT 相位響應特性測試研究

黃銀國　羅小龍　趙美蓉
王毅成　鄭葉龍
天津大學精儀器與光電子工程學院
精密測試技术及儀器國家重點實驗室

摘 要

汽車發動機可變氣門正時（Variable Valve Timing, VVT）可適時調節發動機的進排氣相位，對提高動力性、降低油耗和提高排放性能起著至關重要的作用。優化 VVT 相位響應特性是優化發動機性能的有效途徑。為了設計和優化 VVT，必須通過 VVT 相位響應特性測試來獲得實際的相位響應特性。本文作者设计和介紹了一種 VVT 測試系統。為了得到實際的 VVT 相位響應特性，該測試系統採用了三電機結構，模擬發動機的實際工作環境。在該測試系統中，驅動電機（三相感應電機）模擬發動機的曲軸，負載電機（永磁同步電機，PMSM）作為發動機的凸輪軸。無刷直流電機（BLDC）驅動 VVT。如果採用傳統的比例-積分-微分（PID）控制器，則超調量大，調節時間長。本文作者在常規 PID 控制的基礎上加入了非線性環節，克服了傳統 PID 控制的缺陷。仿真分析和實驗結果表明，採用標準化非線性 PID（SNPID）控制的 VVT 具有較快的相位響應和較小的超調量。